Design of Bimodal Ligands of Neurotensin Receptor 1 for Positron Emission Tomography Imaging and Fluorescence-Guided Surgery of Pancreatic Cancer

Emma Renard, Pierre-Alix Dancer, Christophe Portal, Franck Denat, Aurélie Prignon, Victor Goncalves

Design of Bimodal Ligands of Neurotensin Receptor 1 for PET Imaging and Fluorescence-Guided Surgery of Pancreatic Cancer

Emma Renard,[†] Pierre-Alix Dancer,[#] Christophe Portal,[§] Franck Denat,[†] Aurélie Prignon,[*,‡] and Victor Goncalves[*,†]

[†]Institut de Chimie Moléculaire de l'Université de Bourgogne, UMR CNRS 6302, Université Bourgogne Franche-Comté, 21000, Dijon, France

[#]Kaer Labs, 44300, Nantes, France

[§]Edinburgh Molecular Imaging, EH16 4UX, Edinburgh, United Kingdom

[‡]Sorbonne Université, UMS28, Laboratoire d'Imagerie Moléculaire Positonique (LIMP), 75020, Paris, France

KEYWORDS: Neurotensin; fluorescence-guided surgery; positron emission tomography; dual-modality; gallium-68

ABSTRACT: Neurotensin receptor 1 (NTSR1) is overexpressed in most human pancreatic ductal adenocarcinomas. It makes it an attractive target for the development of pancreatic cancer imaging agents. In this study, we sought to develop a bimodal PET-fluorescent imaging agent capable of specifically targeting these receptors. Starting from the structure of a known NTSR1 agonist, a series of tracers was synthesized, radiometalated with gallium-68 and evaluated *in vitro* and *in vivo,* in mice bearing an AsPC-1 xenograft. PET imaging allowed us to identify the compound [^{68}Ga]Ga-NODAGA-Lys(Cy5**)-AEEAc-[Me-Arg^{8}, Tle^{12}]-NT(7-13) as the one with the most promising biodistribution profile, characterized by high tumor uptake (2.56 ± 0.97 %ID/g, 1 h p.i.) and rapid elimination from non-targeted organs, through urinary excretion. Fluorescence imaging gave similar results. On this basis, fluorescence-guided resection of tumor masses was successfully carried out on a preclinical model.

INTRODUCTION

Pancreatic ductal adenocarcinoma (PDAC), commonly referred to as pancreatic cancer, is the fourth leading cause of death by cancer in Europe.[1,2] This cancer has a poor prognosis, with a survival rate of only 8% at five years, which results from the late clinical presentation of the patients, rapid progression of the disease, and limited efficacy of chemotherapy.[2,3] Only patients with a localized, non-metastatic tumor (10% to 20%), can benefit from surgery. Unfortunately, their selection is difficult because anatomical imaging is weakly effective in detecting local tumor invasion and small metastases. In addition, about 30 to 50% of these patients will relapse.[4] Indeed, the precise evaluation of tumor margins, during surgery or histopathological examination of tissue samples, is challenging, which can lead to incomplete tumor resection. The presence of residual tumor cells after surgery is a strong predictor of tumor recurrence.[5] Therefore, there is a real clinical need to identify new methods that improve both the diagnosis and staging of pancreatic cancer and the accuracy of surgical procedures.

Positron emission tomography (PET) is a nuclear imaging technique that has been widely adopted as a standard tool for diagnosing and staging patients in oncology.[6] PET allows the efficient and quantitative detection of tumors, but suffers from a limited spatial resolution. Fluorescence-guided surgery (FGS) is another fast-growing field which has already achieved clinical success. It relies on fluorescence imaging, a highly resolutive and sensitive imaging modality, which has been shown to improve the quality of tumor resection during the surgical procedure.[7-10]

An attractive strategy for locating primary tumors and their possible metastases is based on the use of bimodal nuclear/optical probes.[11,12] By combining both modalities into a single imaging agent, it is possible to assess the extent of the disease before and after surgery by PET imaging, while fluorescence imaging can be used during surgery to delineate the local spread of the tumor and detect the presence of metastases invisible to the naked eye.

A well-validated marker of pancreatic cancer is neurotensin receptor 1 (NTSR1).[13] NTSR1 is overexpressed in 75-88% of pancreatic adenocarcinomas and high-grade pre-

cancerous lesions (PanINs) but is not detected in healthy pancreas or pancreatitis.[14] Thus, unlike glucose transporters for instance, NTSR1 tracers allow the imaging of malignant pancreatic tumors and related metastases with high specificity.[15-17] Neurotensin (NT) is the endogenous ligand of NTSR1. Its smallest active fragment, NT(8-13), has nanomolar affinity for the receptor.[18,19] Because of its limited half-life *in vivo*, several derivatives were developed to limit proteolytic degradation.[20] A NT(6-13) analog, named NT-20.3, showed an excellent affinity for NTSR1 (IC_{50} = 2.2 ± 0.3 nM).[21] In 2011, Alshoukr *et al*. radiolabeled the peptide NT-20.3 with gallium-68 (^{68}Ga) using DOTA as a chelating agent. This compound showed specific tumor uptake *in vivo*, with high tumor-to-organ ratios, in a model of NTSR1-positive colorectal cancer.[22] These results were further confirmed in 2019 by Prignon *et al*. in subcutaneous and orthotopic models of pancreatic cancer.[23]

To date, only one bimodal PET/fluorescent imaging agent targeting NTSR1 has been reported by the group of Deng and collaborators.[24] This compound, which incorporates a DOTA chelator for copper-64 (^{64}Cu) and a cyanine 5.5 dye, showed a good affinity for the human colon adenocarcinoma cell model, HT-29. Unfortunately, its pharmacokinetic properties are suboptimal, with a significant liver clearance, which was attributed to the hydrophobicity of the fluorophore and/or the release of free ^{64}Cu from the chelator *in vivo*.[25]

In this study, we report the development and evaluation of a series of PET/fluorescent imaging agents targeting NTSR1-positive tumors. These compounds were designed to chelate ^{68}Ga, a positron-emitting radioisotope with a half-life of 67.7 min, well-adapted to the pharmacokinetics of small peptides. Starting from the neurotensin analog NT-20.3, different near-infrared (NIR) fluorescent probes and spacers were tested in order to optimize the biodistribution of the imaging agents. The best compound was validated *in vivo* by PET and NIR fluorescence imaging in mice xenografted with an AsPC-1 model of human pancreatic ductal adenocarcinoma. The selectivity of the imaging agent was further confirmed during the fluorescence-guided resection of tumor masses in the same mouse model.

RESULTS AND DISCUSSION

Design of NTSR1 ligands. A series of bimodal agents was synthesized (Scheme 1). Their structure derives from the sequence of the well-validated peptide agonist NT-20.3 (Ac-Lys-Pro-N-Me-Arg-Arg-Pro-Tyr-Tle-Leu-OH).[21-23,26] A lysine residue was introduced at the *N*-terminal end of the peptide to conjugate the radiometal chelator and the fluorophore, and different spacers were inserted before the lysine: no spacer, a PEG_2 analog (8-amino-3,6-dioxaoctanoic acid, AEEAc) or a PEG_4 chain.

Scheme 1. Synthesis of bimodal NTSR1 ligands

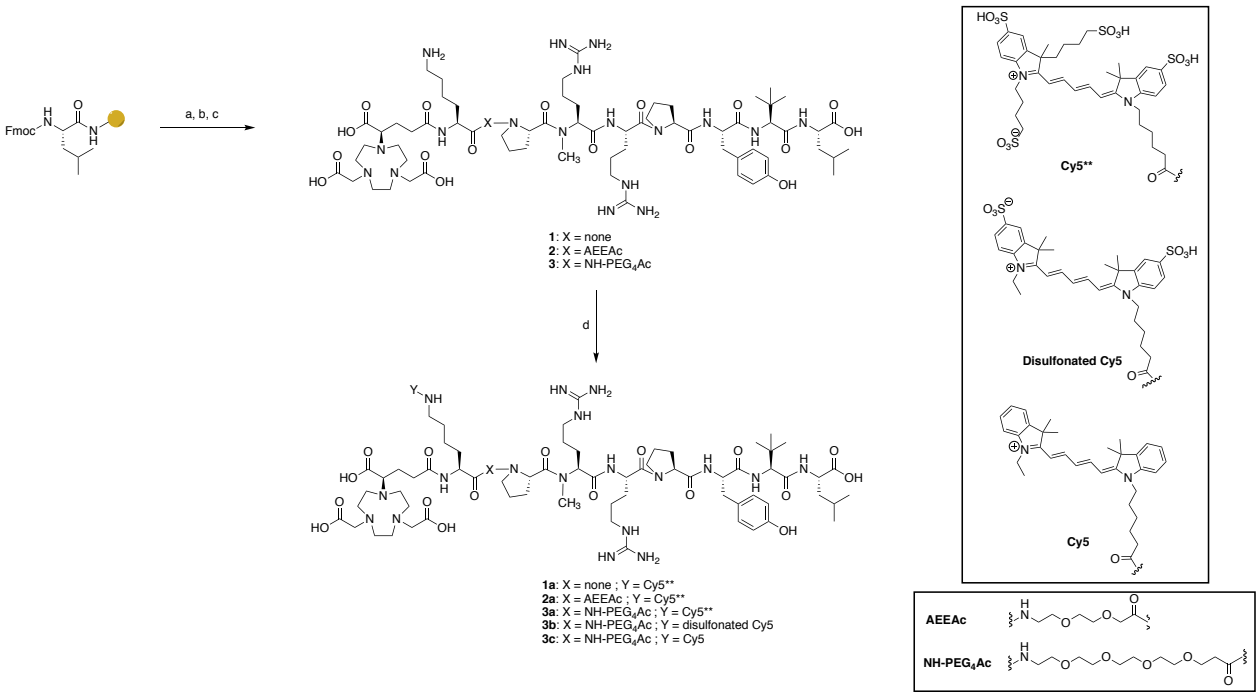

[a]Reagents and conditions: (a) Coupling: Fmoc-(L)-aa(PG)-OH, DIC, Oxyma, DMF, MW. Deprotection: piperidine 20% (*v/v)* in DMF, MW; (b) (*R*)-NODAGA-NHS, DIPEA, DMF, RT, 18 h; (c) TFA/triisopropylsilane/H_2O (95/2.5/2.5, *v/v/v*) RT, 2 h, then 40°C, 4 h; (d) Cy5 derivatives, DIPEA, TSTU, DMF, RT, 20 h. aa: amino acid; PG: protecting group; AEEAc: 8-amino-3,6-dioxaoctanoic acid.

For the PET modality, we chose to use ^{68}Ga among other positron-emitting radioisotopes because its short physical half-life matches well with the rapid pharmacokinetics of peptides, and it provides safer dosimetry for the patients compared to ^{64}Cu.[27] In combination with its good availability, limited cost of operation, and the reliability of commercial ^{68}Ge/^{68}Ga generators, ^{68}Ga is one of the most interesting radioisotopes for PET diagnosis today. (*R*)-NODAGA was chosen as the chelator.[28] This polyazamacrocycle is well-adapted to metals with small ionic radii such as ^{68}Ga and ^{64}Cu.[29] It requires mild radiolabeling conditions and forms highly stable complexes *in vivo*.

For the fluorescent modality, three near-infrared cyanine 5 derivatives, which differ in the number of sulfonate groups, were tested: a cyanine with no sulfonate group (Cy5),[30] a disulfonated cyanine 5,[31-33] and a tetrasulfonated cyanine (Cy5**),[34] which has already shown promising results in a clinical setting.

Synthesis of the ligands. The different bimodal ligands were synthesized in four steps (Scheme 1). First, the peptide was elongated by solid phase peptide synthesis (SPPS), starting from Fmoc-Leu Wang preloaded resin.[35] The different spacers were then introduced at this stage in *N*-terminal position, prior to the coupling of a lysine residue. (*R*)-NODAGA-NHS was then conjugated to the free α-amine of the *N*-terminal lysine. Cleavage and deprotection of the peptides from the resin, followed by RP-HPLC purification of the crude products, afforded compounds **1**, **2**, and **3** in 43% to 69% yield. Finally, the different fluorophores were activated with TSTU and coupled to the ε-amine group of the lysine yielding the NTSR1 ligands **1a**, **2a**, **3a**, **3b**, **3c** in 18% to 48% yield after RP-HPLC purification.

Spectral properties and stability. UV-Vis absorbance and fluorescence spectra were recorded in phosphate buffer (0.01 M) at pH 7.4. The λ_{exc} ranged between 643 and 653 nm and the λ_{em} between 655 and 666 nm, with a Stokes shift of *ca.* 12 nm. No aggregation of the fluorescent dyes was observed in aqueous buffered solution (Figure S9-S11).

The stability of the molecules with regard to enzymatic degradation was then evaluated in mouse serum at 37 °C by RP-HPLC. No significant evolution was observed over 24 h of incubation for the peptides **1a**, **2a**, **3a**, **3b** and **3c** (Figures S18-S22). In contrast, only half of the natural neurotensin was recovered after five hours of incubation in these assay conditions (Figure S17).

***In Vitro* Binding Affinity.** The five compounds were then metalated with ^{nat}Ga. Their K_i was determined in a competition experiment performed on CHO cells overexpressing NTSR1 receptor, using [^{125}I]I-Tyr^3-neurotensin as ligand.[36] All K_i values were close to the one of the reference compound (^{nat}Ga-DOTA-NT-20.3, K_i = 10.0 nM) (Table 1). Interestingly, the spacer appears to play only a minor role in the affinity of ligands for their target, with the exception of the compound bearing a AEEAc chain ^{nat}Ga-**2a**, whose affinity was reduced by a factor of 2 compared to the compounds with no spacer or a PEG$_4$ spacer (^{nat}Ga-**1a** and ^{nat}Ga-**3a** respectively). In contrast, the number of sulfonates had a greater impact on ligand affinity: the absence of sulfonate groups on the cyanine was associated with a stronger binding affinity (K_i of 0.76 nM for the non-sulfonated Cy5 ^{nat}Ga-**3c** *versus* 6.02 nM for the tetrasulfonated Cy5** ^{nat}Ga-**3a**). We hypothesize that these results can be explained by the establishment of non-specific hydrophobic interactions between the Cy5 fluorophore and NTSR1.

Radiolabeling. The compounds were radiolabeled with [^{68}Ga]GaCl$_3$ in sodium acetate buffer (0.8 M, pH 3.5) for 10 min at 40 °C. Radiochemical yields ranged from 51% to 90% and molar activities from 3.5 MBq/nmol to 10.7 MBq/nmol at the end of the radiolabeling (Table S1). The peptides were purified on a C$_{18}$ Sep-Pack cartridge to achieve a radiochemical purity superior to 99% for each tracer, as determined by radio-HPLC analyses. The radiolabeling, quality control and intravenous injection of peptides were completed in less than 1 h. Partition coefficients (LogD) were determined by the shake-flask method in presence of octanol and PBS (0.1 M) at pH 7.4 (Table 1).[37] As expected, the five bimodal agents were all rather hydrophilic. Compounds [^{68}Ga]Ga**1a**, [^{68}Ga]Ga**2a** and [^{68}Ga]Ga**3a** showed the same logD (*ca.* -2.6), suggesting that the hydrophilicity of these molecules is mainly driven by the number of sulfonate groups on the cyanine rather than by the length of the spacer.

Table 1. Inhibition constant and partition coefficient of compounds tested in this study.

Compound	*Ki (nM)* [a]	*LogD* [b]
[$^{nat/68}$Ga]Ga**1a**	5.52 [4.8 – 6.4]	-2.63 ± 0.10
[$^{nat/68}$Ga]Ga**2a**	12.1 [10.3 – 14.2]	-2.51 ± 0.16
[$^{nat/68}$Ga]Ga**3a**	6.02 [4.9 – 7.4]	-2.73 ± 0.13
[$^{nat/68}$Ga]Ga**3b**	3.81 [2.9 – 5.0]	-2.29 ± 0.06
[$^{nat/68}$Ga]Ga**3c**	0.76 [0.66 – 0.88]	-0.70 ± 0.25
[$^{nat/68}$Ga]Ga-DOTA-NT-20.3	10.0 [6.51 – 15.4] [c]	-2.50 ± 0.31

[a] K_i values are presented as "mean [95% confidence interval]" and were determined using ^{nat}Ga-compounds and [^{125}I]I-Tyr^3-neurotensin (0.05 nM, K_d = 0.22 nM) as the radioligand. [b] Partition coefficients (LogD) at pH 7.4 were determined using ^{68}Ga-compounds and are presented as mean ± SD. [c] Alshoukr *et al*. reported an IC$_{50}$ value of 14 ± 2 nM in a competition assay on HT29 cells.[22]

PET Imaging and Biodistribution. In order to assess their pharmacokinetic properties, each radiolabeled bimodal tracer was first injected (473 ± 151 pmol, 3.49 ± 2.71 MBq) into five healthy nude mice. Dynamic PET imaging was performed for 70 min immediately post-injection.

As illustrated in Figure 1, compounds [^{68}Ga]Ga**1a**, [^{68}Ga]Ga**2a**, and [^{68}Ga]Ga**3a** showed a conventional urinary excretion profile, with the majority of the radioactive signal located in the kidneys and bladder. In contrast, compound [^{68}Ga]Ga**3b** also showed signal uptake in the heart and liver, suggesting a longer circulation time in the bloodstream, and clearance of the compound, in part by the hepatic pathway. Finally, the injection of the least hydrophilic compound, [^{68}Ga]Ga**3c,** resulted in significant uptake into the liver. Thus, the presence of four sulfonate groups on the cyanine 5 is essential to achieve a good distribution profile. The length of the spacer did not alter significantly the distribution of this series of NTSR1 ligands.

Thus, further experiments on the tetrasulfonated-compounds ([^{68}Ga]Ga**1a**, [^{68}Ga]Ga**2a** and [^{68}Ga]Ga**3a**) were carried out on a model of human pancreatic adenocarcinoma (AsPC-1), xenografted subcutaneously on the shoulder of nude mice. Static PET images were recorded 40 minutes post-injection of 553 ± 145 pmol, 3.17 ± 0.92 MBq, over 15 minutes (n = 3) (Figure 2A). Tumors were clearly visualized with a high tumor-to-background contrast, even if compound [^{68}Ga]Ga**3a** showed poorer tumor uptake compared to [^{68}Ga]Ga**1a** and [^{68}Ga]Ga**2a**.

In order to confirm these results, an *ex vivo* biodistribution study was performed. One hour after the injection, mice were euthanized, organs were collected, weighed and γ-counted (Table S2). Data showed a clean distribution profile with most of the signal in tumor and kidneys (Figure 2B). The highest uptake was observed in the kidneys with *ca.* 17.5 %ID/g for all three compounds. In agreement with PET data, tumor uptake in compound [^{68}Ga]Ga**3a** was lower (0.95 ± 0.26 %ID/g) than that seen in compounds [^{68}Ga]Ga**1a** and [^{68}Ga]Ga**2a,** with 2.98 ± 0.50 %ID/g and 2.56 ± 0.97 %ID/g respectively (Figure 2B), resulting in lower tumor-to-organ ratios (Figure 2C). To date, we have no clear explanation for the different behavior of [^{68}Ga]Ga**3a** compared to the other two tracers.

Compounds [^{68}Ga]Ga**1a** and [^{68}Ga]Ga**2a** showed a biodistribution profile similar to [^{68}Ga]Ga-DOTA-NT-20.3 apart from a slightly lower signal in the tumor and higher uptake in the kidneys (Table S2).[23] However, tumor-to-blood ratios of compounds [^{68}Ga]Ga**1a** and [^{68}Ga]Ga**2a** were higher than that of [^{68}Ga]Ga-DOTA-NT-20.3 (9.88 ± 2.87, 9.03 ± 2.53 and 5.93 ± 1.82 respectively) (Table S2). Although these values do not reach those obtained with the best ^{68}Ga-PET tracers described in the literature (Prante and co-workers reported a tumor-to-blood ratio of 31 with the NT-peptide tracer [^{68}Ga]Ga**8**, 1 h p.i. on an HT29 model),[38] they remain very satisfactory.[39] In addition, they show that, despite the addition of a fluorescent probe, the biodistribution and affinity for the receptors have not been significantly altered. As expected, almost no uptake was observed in the pancreas, and, unlike the results obtained by Deng *et al.*, liver uptake was minimal.[24]

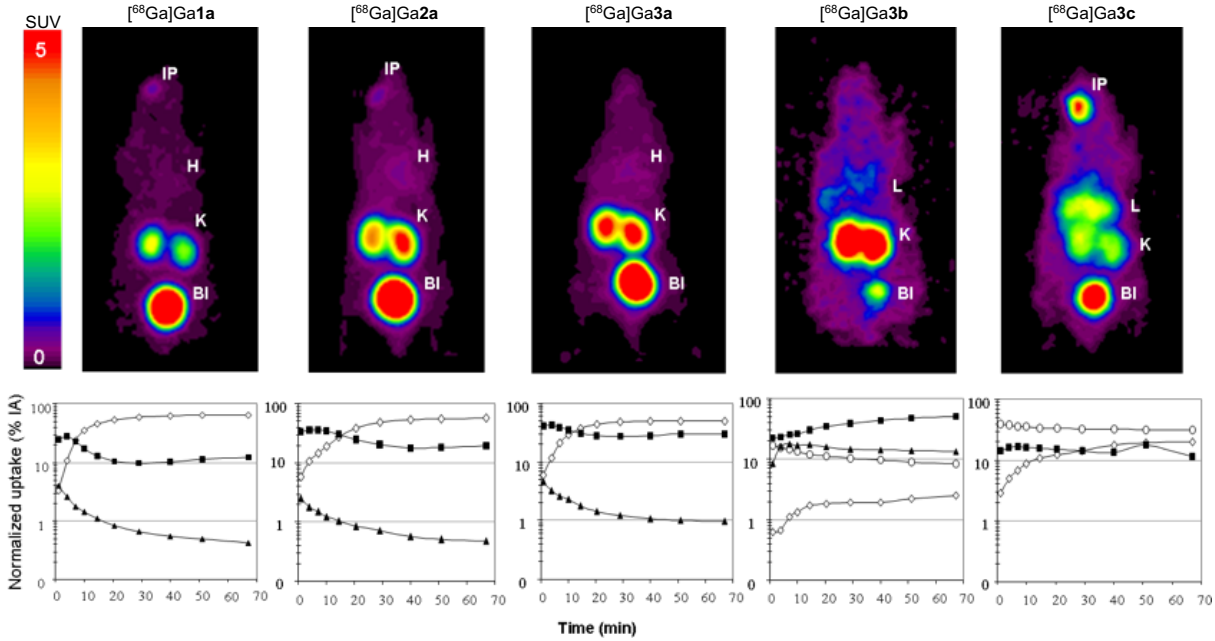

Figure 1. (Top) Maximum intensity projection (MIP) images obtained after 10 min of signal acquisition, between 57-67min p.i., during a dynamic PET imaging study, after the retro-orbitary injection in the sinus vein of [^{68}Ga]Ga**1a**, [^{68}Ga]Ga**2a**, [^{68}Ga]Ga**3a**, [^{68}Ga]Ga**3b** and [^{68}Ga]Ga**3c**. SUV: 3D Standardized Uptake Value data; IP : injection point; H : heart; K : kidneys; Bl : Bladder. (Bottom) Image-derived time activity curves (TACs) for radioactivity in the bladder (open diamonds), kidneys (filled squares), heart (filled triangles) and liver (open circles).

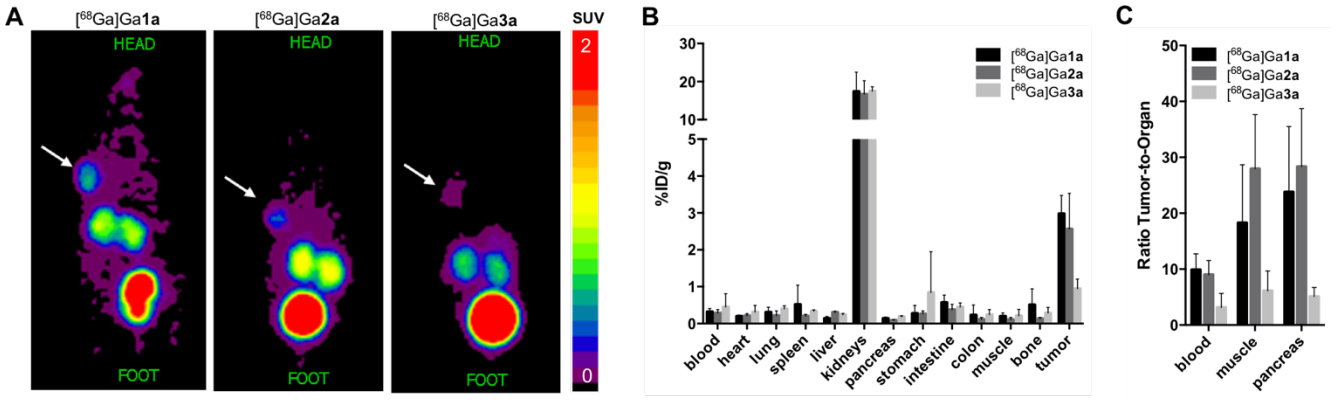

Figure 2. (A) Representative PET images of AsPC-1 tumor-bearing mice. The images show the maximum intensity projections, recorded over 15 min acquisition, 40-55 min p.i. of [^{68}Ga]Ga**1a**, [^{68}Ga]Ga**2a** and [^{68}Ga]Ga**3a**. The location of the xenografted tumor is indicated by a white arrow. (B) Ex vivo biodistribution data of [^{68}Ga]Ga**1a**, [^{68}Ga]Ga**2a** and [^{68}Ga]Ga**3a** 1 h p.i. Values are expressed in percentage of injected dose per gram (%ID/g, mean ± SD) for each collected organ. (C) Tumor-to-organ ratios from ex vivo biodistribution. Data are expressed as means ± SD.

On average, the injection of [^{68}Ga]Ga**2a** resulted in tumor-to-normal tissue ratios higher than [^{68}Ga]Ga**1a** (Figure 2C), which prompted us to select this tracer for the remainder of the study.

Near-Infrared Fluorescence Imaging and Fluorescence-Guided Surgery. Fluorescence images were recorded 1 h, 3 h and 24 h after intravenous administration of different amounts of compound **2a** (50 pmol, 500 pmol and 5 nmol). Mice were euthanized, organs collected, and the uptake of the tracer was quantified by fluorescence imaging at 680 nm (Figure 3, Table S3, Figure S23). In accordance with PET images, the signal was mainly present in the tumor and kidneys. We also noticed fluorescence in the digestive organs, which actually came from the food ingested by the mice. In the other tissues, signal was minimal (Figure 3A).

It is worth noting that the signal in the tumor increased with the injected dose, while it remained about the same in muscles and pancreas. This led to improved tumor-to-muscle and tumor-to-pancreas ratios at the highest tested dose (Figure 3B). The fluorescence signal in tumors decreased substantially over 24 hours, suggesting that fluorescence-guided surgery should ideally be performed within the first few hours post-injection. As shown in Figure 3B, tumor-to-muscle and tumor-to-pancreas ratios of up to 15 could be achieved 1 hour post-injection of a 5 nmol dose of tracer.

Finally, real-time fluorescence imaging was implemented (Supplementary video; Figure 4). This technique allowed the fluorescence-guided resection of tumors in a mouse model. Again, an excellent contrast was found between the tumor and the surrounding healthy tissues.

CONCLUSION

It has been widely established that the nature of the metal, chelator, and even more importantly the fluorophore, can exert a considerable effect on the biodistribution of imaging agents.[28,40]

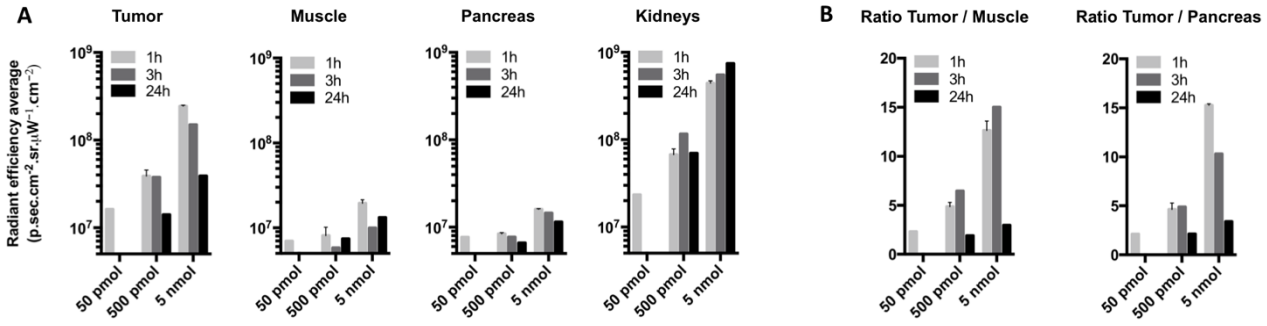

Figure 3. (A) Ex vivo biodistribution of **2a** (50 pmol, 500 pmol and 5 nmol) at 1 h, 3 h and 24 h p.i. by fluorescence imaging. Data are expressed as means of the average radiant efficiency ([p/s/cm²/sr] / [µW/cm²]) for each collected organ. (B) Tumor-to-organ ratios from ex vivo biodistribution. Individual data are available in SI, Table S3. Data could not be collected for the 50 pmol dose at 3 h and 24 h p.i. due to insufficient signal.

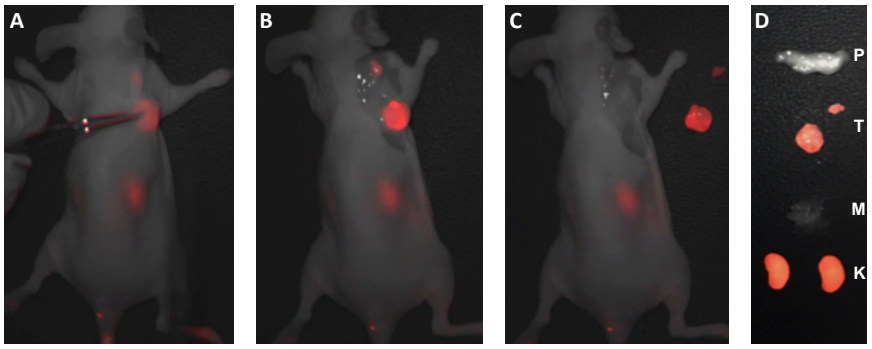

Figure 4. (A-C) Illustrative fluorescence-guided surgery of a mouse bearing an AsPC-1 tumor, 3.5 hours p.i. of **2a** (500 pmol). (D) Fluorescence imaging of isolated organs. P: pancreas, T: tumors, M: muscle, K: kidneys. Images were recorded with an exposure time of 200 ms, a laser excitation at 640 nm and collection of fluorescence emission above 665 nm.

Through the stepwise evaluation of different near-infrared fluorophores and spacers, we were able to identify the tracer [^{68}Ga]Ga**2a**, [^{68}Ga]Ga-NODAGA-Lys(Cy5**)-AEEAc-[Me-Arg^{8}, Tle^{12}]-NT(7-13), as the one with the most interesting distribution, similar to that of [^{68}Ga]Ga-DOTA-NT-20.3. This bimodal compound showed rapid and high tumor uptake, fast clearance from circulation, resulting in high contrast, as early as one hour post injection, both in PET and fluorescence imaging. The accumulation in non-targeted tissues was almost negligible, except in the kidneys/bladder (urinary excretion pathway). Post mortem fluorescence-guided resection confirmed high-contrast fluorescence in the NTSR1-expressing PDAC tumor model and excellent delineation of cancerous cells from surrounding tissues. The evaluation of this tracer on a more relevant orthotopic model of pancreatic cancer is in progress.

While monomodal tracers can be designed for each ap plication, we believe that introducing both modalities into a single agent, at an early stage of drug development, is a more cost-effective approach. Indeed, developing a single new chemical compound should simplify clinical translation and regulatory approval. Furthermore, it guarantees direct correlation between the diagnostic PET images used for surgical planning and the fluorescence images used during tumor resection.

These bimodal tracers should be useful to oncologists, by allowing earlier detection of PDAC primary tumors and small metastases, improving staging procedures, and tailoring of the best therapeutic strategy for each patient. For those who can benefit from surgery, the injection of the non-radioactive fluorescent tracer **2a**, should improve the quality of tumor resection, leading ultimately to increased chances of survival. Future work will focus on the transposition of this dual-labeling strategy to non-peptide antagonists of NTSR1, which exhibit promising biodistribution properties.[41]

EXPERIMENTAL SECTION

All chemicals were purchased from Sigma-Aldrich, Acros Organics and Alfa Aesar and used without further purification. Fmoc-protected amino acids and coupling reagents for peptide synthesis were from Iris Biotech. (*R*)-NODAGA-NHS and DOTA-NHS were provided by CheMatech (Dijon, France). The tetrasulfonated cyanine 5** was kindly given by Dr. Christophe Portal (EM Imaging, Edinburgh, United Kingdom). The disulfonated Cy5 and the Cy5 dye were provided by Pr. Anthony Romieu (ICMUB, Dijon, France). Moisture sensitive reactions were performed under nitrogen or argon atmosphere. The purity of tested compounds was determined by RP-HPLC-MS and was >95%, unless specified. The synthesis of compounds **1, 2, 3** and **2a** is described below. Data for other compounds are available in the Supplementary information document.

Synthesis of peptide conjugates 1, 2, and 3. Peptides were synthesized in 0.1 mmol scale on a Liberty Blue automated microwave peptide synthesizer (CEM, USA). The synthesis was performed by using predefined Fmoc/*t*Bu chemistry protocols on a Fmoc-Leu Wang resin (loading: 0.32 mmol/g), with DIC and Oxyma as coupling agents, and a solution of 20% piperidine in DMF for Fmoc-deprotection steps. A solution of (*R*)-NODAGA-NHS (2 equiv.) and DIPEA (10 equiv.) in dry DMF was added to the resin-bound peptide. The reaction mixture was shaken at room temperature overnight. The resin was washed three times with DMF, CH_2Cl_2 and Et_2O. The peptide was cleaved from the resin using TFA:triisopropylsilane:H_2O (95:2.5:2.5, *v*/*v*/*v*, 5 mL) for 2 h at room temperature. The filtrate was recovered and heated at 40°C for 4 additional hours and then, concentrated under a flow of nitrogen gas, followed by precipitation in diethyl ether and centrifugation (4000 rpm, 10 minutes). The supernatant was removed and the residue was dried under vacuum.

The crude peptide was purified by semi-preparative HPLC on a BetaBasic-18 column (A: H_2O 0.1% TFA, B: MeCN 0.1% TFA with the following gradient program: 10% to 60% of B in 50 min, at a flow rate of 20 mL/min)

and the appropriate fractions were lyophilized to afford target peptides as white powders with a yield ranging from 43 to 69%.

Synthesis of peptide conjugate 2a. To a solution of tetrasulfonated cyanine 5.0 Cy5** (1.3 equiv.) in DMF was added DIPEA (7.8 equiv.) and TSTU (1.3 equiv.). The reaction mixture was stirred at room temperature for 1 h. This solution was added to a solution of peptide (1 equiv.) and DIPEA (10 equiv.) in DMF. The reaction mixture was stirred at room temperature overnight. The solvent was removed under vacuum and the solid was purified by semi-preparative HPLC on a SiliaChrom® dt C_{18} column (Silicycle) (A: TEAB 50 mM, B: MeCN with the following gradient program: 5% of B for 10 min, 5% to 60% of B in 60 min, at a flow rate of 20 mL/min) to afford the target peptide **2a** (triethylammonium salt) as a blue powder (15.8 mg, 23%, purity 94%). HRMS: *m/z* calculated for $C_{109}H_{167}N_{21}O_{33}S_4$ $[M+H]^+$ 2427.09908, found 2427.11013.

***In vitro* stability.** 15 µL of a 5 mM stock solution of peptide in H_2O were stirred in a thermomixer (900 rpm, 37 °C, dark) with 135 µL of mouse serum (Sigma Aldrich, M5905, batch#SLBT4412). The final concentration in peptide was 0.5 mM. After 0 min, 20 min, 35 min, 1 h, 2 h, 4 h, 8 h, and 24 h, a sample (15 µL) was collected and diluted with 60 µL of ethanol 99%. Samples were vortexed and centrifuged (11700 rpm, 10 minutes) to remove precipitated proteins. The supernatant was analyzed by RP-HPLC-MS at a wavelength of 214 nm.

***In vitro* binding affinity.** The affinity of each bimodal compound ^{nat}Ga-**1a**, ^{nat}Ga-**2a**, ^{nat}Ga-**3a**, ^{nat}Ga-**3b** and ^{nat}Ga-**3c** for the NTSR1 receptors was measured on a competitive binding assay on human recombinant CHO cells overexpressing NTSR1, using [^{125}I]I-Tyr^3-neurotensin (0.05 nM, K_d = 0.22 nM) as radioligand (Eurofins, France).[34] IC_{50} values were converted into inhibition constants (K_i) using the Cheng-Prusoff equation.

Radiolabeling. Compounds were radiolabeled using a R&D Synchrom module (Raytest, Germany). The ^{68}Ge/^{68}Ga eluate (1.5 mL, 150–300 MBq) was adjusted to pH 3.5 with sodium acetate (0.8 M). Each compound (9 to 12 nmol; **1a**, **2a**, **3a** as triethylammonium salts; **3b** and **3c** as TFA salts) was added and incubated under agitation at 40 °C for 10 min. The products were purified on a C_{18} Sep-Pack cartridge (Waters Milford, USA) and eluted using 800 µL of 80% ethanol in the second reactor, then subsequently evaporated at 70 °C under argon flow. The final products were diluted with 9 mg/mL sodium chloride (NaCl). HPLC quality control was performed using a reverse-phase column (Discovery Bio, 5 µm, 300 Å, Supelco) on a Waters Breeze System equipped with a 1525 binary pump. Radioactivity was detected with a Berthold radio-HPLC detector. (A: H_2O 0.1% TFA, B: MeCN 0.1% TFA with the following gradient program: 17% to 80% of B in 15 min, at a flow rate of 2 mL/min). The tracers were dissolved in a saline solution (9 mg/mL NaCl) before injection.

Cell culture and animal models. Human pancreatic adenocarcinoma cell line AsPC-1 (ATCC, Rockville, MD, USA) were cultured in RPMI-1640 medium with 10% fetal bovine serum (FBS) in a humidified atmosphere of 5% CO_2 at 37 °C.

All animal experiments were carried out in compliance with the French laws relating to the conduct of animal experimentation. The subcutaneous AsPC-1 tumors were developed by injection of $5x10^6$ cells in a 1:1 mixture of matrigel (BD Biosciences) in the right shoulder of female immunodeficient mice (Nu/nu, Charles River, France) (5-6 weeks old). Animals were subjected to further imaging experiments when the tumors grew to at least 3 mm in diameter.

Small animal PET imaging and biodistribution studies. Healthy female adult Nu/nu mice were weighted and intravenously injected via the retro-orbitary sinus with 3.49 ± 2.71 MBq of each radiotracer based on consistent pmol injected. Dynamic PET imaging was performed immediately p.i. using the Mosaic HP Small Animal Imager (Philips) for 70 min with 4 x 2min, 2 × 5 min frames with 1 min between each sinogram followed by 3 × 10 min frames. The animals were kept under anesthesia using 1.5% of isoflurane from the time of ^{68}Ga-labeled compounds administration until the end of imaging. All sinograms were reconstructed in 3D Standardized Uptake Value (SUV) images and visualized as Maximum Intensity Projection (MIP). Processing of reconstructed images was performed with the Syntegra–Philips software (PETView; Philips Medical Systems). For each mouse submitted to dynamic PET imaging, three-dimensional regions of interest (ROIs) were drawn manually by irregular contouring on PET images as follows: total mouse, heart, kidneys, liver and urinary bladder. The total number of voxels in a given organ was divided by the number of voxels in the "total mouse" for each frame. Data were expressed as normalized uptake in percentage injected activity per organ (% IA) and the decay-corrected mean time-activity curves (TACs) were extracted for each target organ.

Static PET images were acquired at 40 min p.i. for 15 min. After imaging, 1 h p.i. of [^{68}Ga]Ga**1a**, [^{68}Ga]Ga**2a**, [^{68}Ga]Ga**3a** (553 ± 145 pmol, 3.17 ± 0.92 MBq), mice were sacrificed and main organs and tissues were dissected, washed, weighed, and gamma-counted (1480 Wizard 3, Perkin Elmer). Tumor or tissue uptake was expressed as mean ± SD percentage injected dose per gram (%ID/g), corrected for radionuclide decay.

Near-Infrared Fluorescence Imaging. 50 pmol, 500 pmol or 5 nmol of **2a** were injected intravenously, in 0.1 mL volume, in mice bearing subcutaneous AsPC-1 tumors. After 1 h, 3 h or 24 h p.i., optical imaging was conducted *in vivo*,

post mortem with the skin above the tumor removed, and *ex vivo* on dissected tumors and organs using the an IVIS Lumina system (PerkinElmer) with the following settings: 640 ex/680 em (Cy5.5) and 1 sec exposure time. Living Image Software (IVIS Imaging Systems, PerkinElmer) was used to display fluorescence/visible light overlays and measure average radiant efficiencies ([p/s/cm²/sr] / [μW/cm²]) on isolated organs.

Fluorescence-Guided Dissection. The Kaer Imaging System (KIS) 650 (Kaer Labs, Nantes, France) was used for fluorescence real time imaging during the *post mortem* dissection of the tumor. The system has an open design that allows for simultaneous surgery and imaging (open fluorescence). Laser excitation was applied at a wavelength of 640 nm, and fluorescence emission was collected with a high-pass filter with a cut-off frequency of 665 nm. Sequences were saved as series of tiff images with raw data to allow for quantification, before they were exported as movies for illustration. For each fluorescence image, an image with the laser off was subtracted from the fluorescence signal, in order to increase sensitivity and robustness to ambient light. All images (raw fluorescence, background, subtracted images and overlay color images) were displayed in real time and saved.

ASSOCIATED CONTENT

Supporting Information. Materials and general procedures; synthesis and analytical characterization of all compounds; metalation procedure with ^{nat}Ga; *in vitro* stability data; radiolabeling data; tables of *ex vivo* biodistribution data by gamma-counting and fluorescence imaging; additional figures of fluorescence imaging; video of the fluorescence-guided resection of tumors in a mouse model; SMILES formula of each tested compound and associated biochemical data.

This material is available free of charge via the Internet at http://pubs.acs.org.

AUTHOR INFORMATION

Corresponding Authors

*A.P. : aurelie.prignon@sorbonne-universite.fr;

*V.G. : victor.goncalves@u-bourgogne.fr;.

Author Contributions

All authors have given approval to the final version of the manuscript.

Funding Sources

This work was partly funded by the French National Research Agency (ANR) under the French Investissements d'Avenir programs Equipex (IMAPPI, ANR-10-EQPX-05-01), France Life Imaging (FluoNTEP, ANR-11-INBS-0006), and AAP Générique 2017 (ZINELABEL, ANR-17-CE18-0016-01). This work was also supported by the CNRS and the Université de Bourgogne. This work is also part of the project Pharmaco-imagerie et agents théranostiques funded by the Conseil Régional de Bourgogne Franche-Comté through the Plan d'Action Régional pour l'Innovation (PARI) and by the European Union through the PO FEDER-FSE 2014/2020 Bourgogne program.

Notes

The animal study was conducted in accordance with the legislation on the use of laboratory animals (directive 2010/63/EU) and was approved by accredited Ethical committee.

Pierre-Alix Dancer is the co-founder of the company Kaer Labs that develops and sells in vivo fluorescence imaging systems.

ACKNOWLEDGMENT

The authors thank Christophe Piesse from the "Plateforme d'Ingénierie des Protéines de Sorbonne Université, CNRS, Institut de Biologie Paris-Seine, IBPS" for help regarding the synthesis protocol of NT-20.3 and Aurélien Gibier for the synthesis of DOTA-NT-20.3. We also thank the "Plateforme d'Analyse Chimique et de Synthèse Moléculaire de l'Université de Bourgogne" (http://www.wpcm.fr) for access to analytical instrumentation and Pr. Anthony Romieu for providing Cy5 and the disulfonated cyanine 5.

ABBREVIATIONS

AEEAc, 8-amino-3,6-dioxaoctanoic acid; CHO, Chinese hamster ovary; Cy5, Cyanine 5; DOTA, 1,4,7,10-tetraazacyclododecane-1,4,7,10-tetraacetic acid; FGS, fluorescence-guided surgery; NIR, near infra-red; (*R*)-NODAGA, (*R*)-1,4,7-triazacyclononane,1-glutaric acid-4,7-acetic acid; NT, neurotensin; NTSR1, neurotensin receptor 1; PBS, Phosphate buffer saline; PDAC, pancreatic ductal adenocarcinoma; PET, positron emission tomography; TEAB, Triethylammonium bicarbonate.

REFERENCES

(1) Carrato, A.; Falcone, A.; Ducreux, M.; Valle, J. W.; Parnaby, A.; Djazouli, K.; Alnwick-Allu, K.; Hutchings, A.; Palaska, C.; Parthenaki, I. A Systematic Review of the Burden of Pancreatic Cancer in Europe: Real-World Impact on Survival, Quality of Life and Costs. *J. Gastrointest. Canc.* **2015,** *46*, 201-211.

(2) Hidalgo, M.; Cascinu, S.; Kleeff, J.; Labianca, R.; Lohr, J. M.; Neoptolemos, J.; Real, F. X.; Van Laethem, J. L.; Heinemann, V. Addressing the Challenges of Pancreatic Cancer: Future Directions for Improving Outcomes. *Pancreatology* **2015,** *15*, 8-18.

(3) Saad, A. M.; Turk, T.; Al-Husseini, M. J.; Abdel-Rahman, O. Trends in Pancreatic Adenocarcinoma Incidence and Mortality in the United States in the Last Four Decades; a SEER-Based Study. *BMC Cancer* **2018,** *18*, 688.

(4) La Torre, M.; Nigri, G.; Lo Conte, A.; Mazzuca, F.; Tierno, S. M.; Salaj, A.; Marchetti, P.; Ziparo, V.; Ramacciato, G. Is a Preoperative Assessment of the Early Recurrence of Pancreatic Cancer Possible After Complete Surgical Resection? *Gut Liver* **2014,** *8*, 102-108.

(5) Neoptolemos, J. P.; Stocken, D. D.; Dunn, J. A.; Almond, J.; Beger, H. G.; Pederzoli, P.; Bassi, C.; Dervenis, C.; Fernandez-Cruz, L.; Lacaine, F.; Buckels, J.; Deakin, M.; Adab, F. A.; Sutton, R.; Imrie, C.; Ihse, I.; Tihanyi, T.; Olah, A.; Pedrazzoli, S.; Spooner, D.; Kerr, D. J.; Friess, H.; Buchler, M. W. Influence of Resection Margins on Survival for Patients with Pancreatic Cancer Treated by Adjuvant Chemoradiation and/or

Chemotherapy in the ESPAC-1 Randomized Controlled Trial. *Ann. Surg.* **2001,** *234*, 758-768.

(6) Vaquero, J. J.; Kinahan, P. Positron Emission Tomography: Current Challenges and Opportunities for Technological Advances in Clinical and Preclinical Imaging Systems. *Annu. Rev. Biomed. Eng.* **2015,** *17*, 385-414.

(7) Nagaya, T.; Nakamura, Y. A.; Choyke, P. L.; Kobayashi, H. Fluorescence-Guided Surgery. *Front. Oncol.* **2017,** *7*, 314.

(8) Hernandez Vargas, S.; Ghosh, S. C.; Azhdarinia, A. New Developments in Dual-Labeled Molecular Imaging Agents. *J. Nucl. Med.* **2019,** *60*, 459-465.

(9) Xi, L.; Jiang, H. Image-Guided Surgery Using Multimodality Strategy and Molecular Probes. *Wiley Interdiscip. Rev. Nanomed. Nanobiotechnol.* **2016,** *8*, 46-60.

(10) Zhao, J.; Chen, J.; Ma, S.; Liu, Q.; Huang, L.; Chen, X.; Lou, K.; Wang, W. Recent Developments in Multimodality Fluorescence Imaging Probes. *Acta Pharm. Sin. B* **2018,** *8*, 320-338.

(11) Seibold, U.; Wängler, B. r.; Schirrmacher, R.; Wängler, C. Bimodal Imaging Probes for Combined PET and OI: Recent Developments and Future Directions for Hybrid Agent Development. *BioMed Res. Int.* **2014**, 13 pages.

(12) Azhdarinia, A.; Ghosh, P.; Ghosh, S.; Wilganowski, N.; Sevick-Muraca, E. M. Dual-Labeling Strategies for Nuclear and Fluorescence Molecular Imaging: a Review and Analysis. *Mol. Imaging Biol.* **2012,** *14*, 261-276.

(13) Wu, Z.; Martinez-Fong, D.; Tredaniel, J.; Forgez, P Neurotensin and its High Affinity Receptor 1 as a Potential Pharmacological Target in Cancer Therapy. *Front. Endocrinol.* **2013,** *3*.

(14) Körner, M.; Waser, B.; Strobel, O.; Büchler, M.; Reubi, J. C. Neurotensin Receptors in Pancreatic Ductal Carcinomas. *EJNMMI Res.* **2015,** *5*, 17.

(15) Reubi, J. C.; Waser, B.; Friess, H.; Buchler, M.; Laissue, J. Neurotensin Receptors: a New Marker for Human Ductal Pancreatic Adenocarcinoma. *Gut.* **1998,** *42*, 546-550.

(16) Yin, X.; Wang, M.; Wang, H.; Deng, H.; He, T.; Tan, Y.; Zhu, Z.; Wu, Z.; Hu, S.; Li, Z. Evaluation of Neurotensin Receptor 1 as a Potential Imaging Target in Pancreatic Ductal Adenocarcinoma. *Amino Acids* **2017,** *49*, 1325-1335.

(17) De Visser, M.; Janssen, P. J.; Srinivasan, A.; Reubi, J. C.; Waser, B.; Erion, J. L.; Schmidt, M. A.; Krenning, E. P.; De Jong, M. Stabilised 111In-Labelled DTPA- and DOTA-Conjugated Neurotensin Analogues for Imaging and Therapy of Exocrine Pancreatic Cancer. *Eur. J. Nucl. Med. Mol. Imaging* **2003,** *30*, 1134-1139.

(18) Krumm, B. E.; Lee, S.; Bhattacharya, S.; Botos, I.; White, C. F.; Du, H.; Vaidehi, N.; Grisshammer, R. Structure and Dynamics of a Constitutively Active Neurotensin Receptor. *Sci. Rep.* **2016**.

(19) Myers, R. M.; Shearman, J. W.; Kitching, M. O.; Ramos-Montoya, A.; Neal, D. E.; Ley, S. V. Cancer, Chemistry, and the Cell: Molecules that Interact with the Neurotensin Receptors. *ACS Chem. Biol.* **2009,** *4*, 503-525.

(20) Kokko, K. P.; Hadden, M. K.; Orwig, K. S.; Mazella, J.; Dix, T. A. In Vitro Analysis of Stable, Receptor-Selective Neurotensin[8−13] Analogues. *J. Med. Chem.* **2003,** *46*, 4141-4148.

(21) Alshoukr, F.; Rosant, C.; Maes, V.; Abdelhak, J.; Raguin, O.; Burg, S.; Sarda, L.; Barbet, J.; Tourwé, D.; Pelaprat, D.; Gruaz-Guyon, A. Novel Neurotensin Analogues for Radioisotope Targeting to Neurotensin Receptor-Positive Tumors. *Bioconjugate Chem.* **2009,** *20*, 1602-1610.

(22) Alshoukr, F.; Prignon, A.; Brans, L.; Jallane, A.; Mendes, S.; Talbot, J.-N.; Tourwé, D.; Barbet, J.; Gruaz-Guyon, A. Novel DOTA-Neurotensin Analogues for 111In Scintigraphy and 68Ga PET Imaging of Neurotensin Receptor-Positive Tumors. *Bioconjugate Chem.* **2011,** *22*, 1374-1385.

(23) Prignon, A.; Provost, C.; Alshoukr, F.; Wendum, D.; Couvelard, A.; Barbet, J.; Forgez, P.; Talbot, J.-N.; Gruaz-Guyon, A. Preclinical Evaluation of 68Ga-DOTA-NT-20.3: A Promising PET Imaging Probe To Discriminate Human Pancreatic Ductal Adenocarcinoma from Pancreatitis. *Mol. Pharmaceutics* **2019,** *16*, 2776-2784.

(24) Deng, H.; Wang, H.; Wang, M.; Li, Z.; Wu, Z. Synthesis and Evaluation of 64Cu-DOTA-NT-Cy5.5 as a Dual-Modality PET/Fluorescence Probe to Image Neurotensin Receptor-Positive Tumor. *Mol. Pharmaceutics* **2015,** *12*, 3054-3061.

(25) Dearling, J. L. J.; Voss, S. D.; Dunning, P.; Snay, E.; Fahey, F.; Smith, S. V.; Huston, J. S.; Meares, C. F.; Treves, S. T.; Packard, A. B. Imaging Cancer Using PET-the Effect of the Bifunctional Chelator on the Biodistribution of a (64)Cu-Labeled Antibody. *Nucl. Med. Biol.* **2011,** *38*, 29-38.

(26) Marenco, M.; Lodola, L.; Persico, M. G.; Frangipane, V.; Facoetti, A.; Aprile, C.; Hodolic, M. Evidence of (68)Ga-DOTA-NT-20.3 Uptake in Pancreatic Adenocarcinoma AsPC-1 Cell Line - in vitro Study. *Curr. Pharm. Biotechnol.* **2018,** *19*, 754-759.

(27) Brandt, M.; Cardinale, J.; Aulsebrook, M. L.; Gasser, G.; Mindt, T. L. An Overview of PET Radiochemistry, Part 2: Radiometals. *J. Nucl. Med.* **2018,** *59*, 1500-1506.

(28) Fani, M.; Del Pozzo, L.; Abiraj, K.; Mansi, R.; Tamma, M. L.; Cescato, R.; Waser, B.; Weber, W. A.; Reubi, J. C.; Maecke, H. R. PET of Somatostatin Receptor–Positive Tumors Using 64Cu- and 68Ga-Somatostatin Antagonists: The Chelate Makes the Difference. *J. Nucl. Med.* **2011,** *52*, 1110-1118.

(29) Gourni, E.; Canovas, C.; Goncalves, V.; Denat, F.; Meyer, P. T.; Maecke, H. R. (R)-NODAGA-PSMA: A Versatile Precursor for Radiometal Labeling and Nuclear Imaging of PSMA-Positive Tumors. *PLoS One* **2015,** *10*, e0145755.

(30) Pisoni, D. S.; Todeschini, L.; Borges, A. C. A.; Petzhold, C. L.; Rodembusch, F. S.; Campo, L. F. Symmetrical and Asymmetrical Cyanine Dyes. Synthesis, Spectral Properties, and BSA Association Study. *J. Org. Chem.* **2014,** *79*, 5511-5520.

(31) Mujumdar, R. B.; Ernst, L. A.; Mujumdar, S. R.; Lewis, C. J.; Waggoner, A. S. Cyanine Dye Labeling Reagents: Sulfoindocyanine Succinimidyl Esters. *Bioconjugate Chem.* **1993,** *4*, 105-111.

(32) Canovas, C.; Moreau, M.; Bernhard, C.; Oudot, A.; Guillemin, M.; Denat, F.; Goncalves, V. Site-Specific Dual Labeling of Proteins on Cysteine Residues with Chlorotetrazines. *Angew. Chem. Int. Ed.* **2018,** *57*, 10646-10650.

(33) Canovas, C.; Moreau, M.; Vrigneaud, J. M.; Bellaye, P. S.; Collin, B.; Denat, F.; Goncalves, V. Modular Assembly of Multimodal Imaging Agents through an Inverse Electron Demand Diels-Alder Reaction. *Bioconjugate Chem.* **2019,** *30*, 888-897.

(34) Burggraaf, J.; Kamerling, I. M.; Gordon, P. B.; Schrier, L.; de Kam, M. L.; Kales, A. J.; Bendiksen, R.; Indrevoll, B.; Bjerke, R. M.; Moestue, S. A.; Yazdanfar, S.; Langers, A. M.; Swaerd-Nordmo, M.; Torheim, G.; Warren, M.; Morreau, H.; Voorneveld, P.; Buckle, T.; van Leeuwen, F. W.; Odegardstuen, L. I.; Dalsgaard, G. T.; Healey, A.; Hardwick, J. C. Detection of Colorectal Polyps in Humans Using an Intravenously

Administered Fluorescent Peptide Targeted Against c-Met. *Nat. Med.* **2015,** *21*, 955-961.

(35) Coin, I.; Beyermann, M. Bienert, M. Solid-Phase Peptide Synthesis: from Standard Procedures to the Synthesis of Difficult Sequences. *Nat. Protoc.* **2007,** *2*, 3247-3256.

(36) Vita, N.; Laurent, P. Lefort, S.; Chalon, P.; Dumont, X.; Kaghad, M.; Gully, D.; Le Fur, G.; Ferrara, P.; Caput, D. Cloning and Expression of a Complementary DNA Encoding a High Affinity Human Neurotensin Receptor. *FEBS Lett.* **1993,** *317*, 139-142.

(37) Andrés, A.; Rosés, M.; Ràfols, C.; Bosch, E.; Espinosa, S.; Segarra, V.; Huerta, J. M. Setup and Validation of Shake-Flask Procedures for the Determination of Partition Coefficients (logD) from Low Drug Amounts. *Eur. J. Pharm. Sci.* **2015,** *76*, 181-191.

(38) Maschauer, S.; Einsiedel, J.; Hübner, H.; Gmeiner, P.; Prante, O. 18F- and 68Ga-Labeled Neurotensin Peptides for PET Imaging of Neurotensin Receptor 1. *J. Med. Chem.* **2016,** *59*, 6480-6492.

(39) Maschauer, S.; Ruckdeschel, T.; Tripal, P.; Haubner, R.; Einsiedel, J.; Hübner, H.; Gmeiner, P.; Kuwert, T.; Prante, O. In Vivo Monitoring of the Antiangiogenic Effect of Neurotensin Receptor-Mediated Radiotherapy by Small-Animal Positron Emission Tomography: A Pilot Study. *Pharmaceuticals* **2014,** *7*, 464-481.

(40) Bunschoten, A.; van Willigen, D. M.; Buckle, T.; van den Berg, N. S.; Welling, M. M.; Spa, S. J.; Wester, H.-J.; van Leeuwen, F. W. B. Tailoring Fluorescent Dyes To Optimize a Hybrid RGD-Tracer. *Bioconjugate Chem.* **2016,** *27*, 1253-1258.

(41) Schulz, J.; Rohracker, M.; Stiebler, M.; Goldschmidt, J.; Grosser, O. S.; Osterkamp, F.; Pethe, A.; Reineke, U.; Smerling, C.; Amthauer, H. Comparative Evaluation of the Biodistribution Profiles of a Series of Nonpeptidic Neurotensin Receptor-1 Antagonists Reveals a Promising Candidate for Theranostic Applications. *J. Nucl. Med.* **2016,** *57*, 1120-1123.

Table of Contents Graphic